

Robust Multi-Carrier, Multi-Satellite Vector Phase Locked Loop with Wideband Ionospheric Correction and Integrated Weighted RAIM

Patrick Henkel*, Grace Xingxin Gao**, Todd Walter** and Christoph Günther*,***

**Technische Universität München, Munich, Germany*

***Stanford University, Stanford, USA*

****German Aerospace Center (DLR), Oberpfaffenhofen, Germany*

BIOGRAPHIES

Patrick Henkel studied electrical engineering and information technology at the Technische Universität München, Germany and the École Polytechnique de Montréal, Canada. He is a Ph.D. student at the Institute of Communications and Navigation at TUM since 2005 and focuses on robust ambiguity resolution for precise carrier phase positioning with multiple frequencies. In 2007, he was a guest researcher at TU Delft and won the Pierre Contensou Gold Medal at the International Astronautical Congress. In 2008, he received a DAAD fellowship for a research visit of the GPS lab at Stanford University where he worked on wideband ionospheric corrections for multi-carrier, multi-satellite vector phase locked loops.

Grace Xingxin Gao is a research associate at Stanford University. She received her B.S. in Mechanical Engineering in 2001 and her M.S. in Electrical Engineering in 2003, both from Tsinghua University, Beijing, China. She received the Ph.D. for her thesis entitled “Towards navigation based on 120 satellites: Analyzing the new signals” from Stanford University in 2008. She is also the recipient of the “2008 Young Achievement Award” from the Institute of Navigation. Her current research interests include Galileo signal and code structures, GNSS receiver architectures, and GPS modernization.

Todd Walter is the director of the Wide Area Augmentation System (WAAS) Laboratory in the department of Aeronautics and Astronautics at Stanford University. He has received his Ph.D. from Stanford University in 1993. He is a fellow of the ION, has co-authored more than 120 papers, and received the Thurlow award for his contributions to satellite navigation, including education, aviation applications and the mitigation of ionospheric effects in 2008. His current research interests include the development of WAAS integrity algorithms and the availability analysis of the WAAS signals.

Christoph Günther studied theoretical physics at the Swiss Federal Institute of Technology in Zurich. He received his diploma in 1979 and completed his Ph.D. in 1984. He worked on communication and information theory at Brown Boveri and Ascom Tech. From 1995, he led the development of mobile phones for GSM and later dual mode GSM/Satellite phones at Ascom. In 1999, he became head of the research department of Ericsson in Nuremberg. Since 2003, he is the director of the Institute of Communication and Navigation at the German Aerospace Center (DLR) and since December 2004, he additionally holds a Chair at the Technische Universität München. His research interests are in satellite navigation, communication, and signal processing.

ABSTRACT

Current GNSS receivers have independent Phase Locked Loops (PLLs) for each satellite and frequency. The introduction of new GPS signals on L5 and the development of new satellite constellations (Galileo, Compass) increases the number of PLLs and, thus, the probability of a loss of lock of one PLL. This probability becomes especially critical during ionospheric scintillations with frequent deep amplitude fades of more than 20 dB. The outage of a PLL on one frequency prevents the computation of an ionosphere-free combination at this instant, and thus, degrades the positioning accuracy.

Therefore, a Multi-Carrier, Multi-Satellite Vector-PLL (MC-MS-VPLL) has been recently suggested to improve both accuracy and robustness of carrier tracking. The individual PLLs are coupled by transforming the tracking errors at the discriminator outputs into a position drift, a clock drift, ionospheric drifts and tropospheric drifts. These quantities are fed into loop filters whose bandwidths are adapted to the dynamics of the receiver, of its clock and of the atmospheric delays. The MC-MS-VPLL assigns a low weight to satellites during deep amplitude fades and a high weight for a high power level. This enables robust carri-

er tracking even during severe ionospheric scintillations as the stronger signals are helping to track the weaker signals.

There exist two threats of a MC-MS-VPLL that are addressed in this paper: The first one is ionospheric dispersion within the wideband Galileo E5 signal (51 MHz bandwidth) which causes ripples in the code signal and a power shift in correlation result from the real part to the imaginary part. If no wideband correction is applied, the phase tracked by an independent PLL is biased by 14° for 100 TECU, and this bias can not be mapped to the ionospheric delay tracked by a MC-MS-VPLL. A correction term is derived for the mitigation of these wideband ionospheric effects. Secondly, the joint tracking means that any failure on one or more satellites or frequencies (e.g. phase jump on satellite clock, low elevation multipath) affects the tracking of all satellites and frequencies. A Receiver Autonomous Integrity Monitoring (RAIM) is integrated into the MC-MS-VPLL to detect and exclude severely biased satellites from the joint tracking. The weighted sum of squared error test statistic is computed from the carrier tracking errors given by the discriminator outputs.

INTRODUCTION

The joint tracking of all satellites goes back to Spilker who has proposed a Vector Delay Locked Loop (DLL) for code delay tracking in [1]. The tracking errors were originally transformed into a position drift and a clock drift by weighted least-square estimation which does not consider ionospheric and tropospheric delays and other biases like multipath as individual parameters. The benefit of the VDLL is the adaptive weighting of satellites, i.e. the stronger signals help to track the weaker signals. The vector tracking of carrier phase is more challenging due to its higher precision and the existence of an unknown integer ambiguity for each satellite and frequency.

Zhodzishsky, Yudanov, Veitsel and Ashjaee have first applied vector tracking to carrier phase in [2]. The tracking errors at the discriminator outputs were transformed into position errors and clock drifts by weighted least-square estimation. The atmospheric delays were not considered as individual parameters in the filtering which motivated Zhodzishsky et al. to use both individual and joint loop filters, and to combine both results in the oscillators. They attempted to separate the parameters by different filter bandwidths, i.e. a large bandwidth was chosen for the position and clock filters due to its higher dynamics and a small bandwidth was selected for the individual loop filters. However, the atmospheric errors are also present in the position and clock filters, and the position and clock drifts also occur to a certain degree in the individual filters. Consequently, this “Co-Op tracking” reduces the tracking error of an individual PLL but is still sub-optimal as the physically different error sources are not completely separated.

In the MC-MS-VPLL of [3], the authors have coupled

individual PLLs by transforming the tracking errors of the discriminator outputs into a position drift, a receiver clock drift, ionospheric delay drifts and a tropospheric zenith delay drift. These quantities are fed into loop filters whose bandwidths are adapted to the dynamics of the receiver, of its clock and of the ionospheric and tropospheric delays. Note that the MC-MS-VPLL is not limited to measurements from a single constellation. The joint tracking of satellites from multiple constellations further improves the tracking performance as position drift, clock drift and tropospheric zenith delay drift are equal for all constellations. The MC-MS-VPLL can also be extended to include measurements from several antennas.

The objectives of this paper are two-fold: First, two strategies are proposed to mitigate the wideband ionospheric effects that have been analysed by Gao et al. in [4]. Both require an estimate of the ionospheric delay which is not biased by wideband ionospheric effects. The ionospheric dispersion within the E5 band results in a complex correlation result which shifts the phase but does not cause an additional delay in the estimated code delay. Thus, the intra-band ionospheric dispersion differs from the classical code-carrier divergence which motivates the computation of the ionospheric delay from a linear combination of code measurements. The estimated ionospheric delay at a given reference frequency enables the computation of a phase shift for each frequency, and thus the equalization of wideband ionospheric effects in frequency domain. This method requires an FFT of the downconverted signal and an IFFT after the application of the wideband correction. Alternatively, the phase correction can be determined from a look-up table and applied before the tracking, which improves the efficiency of the first method as it does not require the FFT and IFFT. It is shown that the phase correction increases linearly with the TEC, and that the gradient of the phase correction w.r.t. TEC equals $8^\circ/100$ TECU for a bandwidth of 30 MHz and $14^\circ/100$ TECU for a bandwidth of 50 MHz. These rather low gradients indicate that a rough estimate of TEC (± 5 TECU) is sufficient to correct wideband ionospheric effects.

The second threat of a VPLL (multipath and other failures affecting a subset of satellites or frequencies) requires the integration of a fault detection method. The weighted RAIM of Walter and Enge [5] has been chosen due to its efficiency. Large phase jumps on one or more satellites result in an unstable behaviour of the MC-MS-VPLL as the phase errors can not be mapped into one of the tracked parameters (position, clock drift, ionospheric and tropospheric delays). Another error might occur in the weighting matrix which partially compensates the gain obtained from the joint tracking. It is shown that the MC-MS-VPLL achieves a lower tracking error than independent tracking loops even if the low elevation satellites suffer from an up to five times larger standard deviation than considered in the weighting matrix. For fault detection, a Weighted Sum

of Squared Error (WSSE) test statistic is computed from the range residuals using the discriminator outputs. This WSSE is related to the average WSSE in the absence of biases, e.g. due to multipath. The ratio is called WSSE amplification due to multipath and it enables the detection of a failure if a predefined threshold is exceeded. It is shown that the WSSE is very sensitive to multipath and that the WSSE amplification is substantially larger than the amplification of the standard deviation of the estimated phase. Therefore, a failure can already be detected when the benefit of joint tracking is still larger than the degradation due to an erroneous weighting matrix. WSSE amplification of up to 100 has been observed for severe multipath from a single reflector. Moreover, protection levels are computed from the discriminator outputs in the presence of multiple biases. The HPL and VPL depend on the largest position biases that do not exceed the threshold of the WSSE test statistics for a given probability of false alert.

PRINCIPLES OF VECTOR PHASE LOCKED LOOP

Fig. 1 shows the functional diagram of a Multi-Carrier Single-Satellite (MC-SS)-VPLL. The received signal $r_m(t_i)$ on frequency $m \in \{1, \dots, M\}$ at time instant t_i is modeled in baseband as

$$r_m(t_i) = x(\tilde{t}_m - \tau_m) \cdot e^{-j\phi_m(t_i)} + \eta_m(t_i), \quad (1)$$

with the code signal $x(\tilde{t}_m - \tau_m)$, the code delay τ_m , the received phase $\phi_m(t_i)$ and the noise $\eta_m(t_i)$. The received signal is multiplied by the oscillator generated signal $e^{j\hat{\phi}_m(t_i)}$, and correlated with a local copy of the code signal $x(\tilde{t}_m - \hat{\tau}_m)$. The non-linear discriminators (see Kaplan and Hegarty [6]) extract the carrier tracking errors $\Delta\phi_m(t_i) = \phi_m(t_i) - \hat{\phi}_m(t_i)$ from the correlation result. The tracking errors are modeled as

$$\begin{bmatrix} \Delta\phi_1(t_i) \\ \vdots \\ \Delta\phi_M(t_i) \end{bmatrix} = \mathbf{X} \cdot \begin{bmatrix} \Delta\tilde{r}(t_i) \\ \Delta I(t_i) \end{bmatrix} + \Delta\varepsilon(t_i), \quad (2)$$

with

$$\mathbf{X} = \begin{bmatrix} 1 & q_{11}^2 & & \\ \vdots & & \ddots & \\ 1 & & & q_{1M}^2 \end{bmatrix}, \quad (3)$$

the ratio of frequencies $q_{1m} = f_1/f_m$ and $\Delta\varepsilon = \mathcal{N}(\mathbf{0}, \Sigma)$. The range error $\Delta\tilde{r}(t_i)$ including all non-dispersive error sources (e.g. clock offsets and tropospheric delay) and the ionospheric error $\Delta I(t_i)$ at a reference frequency are determined from the discriminator outputs by weighted least-square estimation, i.e.

$$\begin{bmatrix} \Delta\hat{r}(t_i) \\ \Delta\hat{I}(t_i) \end{bmatrix} = \mathbf{S} \cdot \begin{bmatrix} \Delta\phi_1(t_i) \\ \vdots \\ \Delta\phi_M(t_i) \end{bmatrix} \quad (4)$$

with

$$\mathbf{S} = \left(\mathbf{X}^T \Sigma^{-1} \mathbf{X} \right)^{-1} \mathbf{X}^T \Sigma^{-1}. \quad (5)$$

The estimates $\Delta\hat{r}(t_i)$ and $\Delta\hat{I}(t_i)$ are filtered by \mathbf{F} , then transformed back into phase tracking errors by \mathbf{X} , and accumulated over time to obtain the phases $\hat{\phi}_m(t_i)$.

This MC-SS-VPLL and a more generalized Multi-Carrier, Multi-Satellite (MC-MS)-VPLL have been proposed by Henkel, Giger and Günther in [3]. It substantially increases the robustness of carrier tracking over jamming, ionospheric scintillations and carrier phase multipath. It can achieve the same tracking error as an individual PLL but at a more than 10 dB lower carrier to noise power ratio. It is recommended to initialize any VPLL by independent PLLs to avoid the estimation of phase biases and integer ambiguities. Therefore, the switches in Fig. 1 are first brought in the upper position. As soon as the phases on two frequencies are locked, the joint tracking is turned on.

Fig. 2 shows a MC-MS-VPLL where the code correlation has been omitted to simplify the notation. An orthogonal projection is applied to the carrier tracking errors to eliminate the clock drift, the ionospheric and tropospheric delays. Let us introduce the following matrices for the mapping of the position, clock offset, ionospheric delays and tropospheric wet zenith delay into range domain:

$$\begin{aligned} \mathbf{X}_x &= \mathbf{1}^{M \times 1} \otimes \left[\mathbf{e}^{(1),T}, \dots, \mathbf{e}^{(K),T} \right]^T \\ \mathbf{X}_{\delta\tau} &= \mathbf{1}^{KM \times 1} \\ \mathbf{X}_I &= [q_{11}^2, \dots, q_{1M}^2]^T \otimes \mathbf{1}^{K \times K} \\ \mathbf{X}_T &= \mathbf{1}^{M \times 1} \otimes \left[m_w^{(1)}, \dots, m_w^{(K)} \right]^T, \end{aligned} \quad (6)$$

with the Kronecker product \otimes , the unit vectors $\mathbf{e}^{(k)}$ pointing from satellite $k \in \{1, \dots, K\}$ to the receiver, and the mapping function m_w for the tropospheric zenith delay. The matrices of the nuisance parameters are combined to

$$\mathbf{X}_{\bar{x}} = [\mathbf{X}_{\delta\tau}, \mathbf{X}_I, \mathbf{X}_T], \quad (7)$$

and an orthogonal projector is computed for the position:

$$P_{\bar{\mathbf{X}}_x}^\perp = \mathbf{1}^{KM \times KM} - \mathbf{X}_{\bar{x}} \left(\mathbf{X}_{\bar{x}}^T \Sigma^{-1} \mathbf{X}_{\bar{x}} \right)^{-1} \mathbf{X}_{\bar{x}}^T \Sigma^{-1}, \quad (8)$$

which eliminates the drifts of the clock offset and atmospheric delays. The least-square estimate of the position drift has been determined by Teunissen in [7] as

$$\Delta\hat{x} = P_x \Delta\phi = \left(\bar{\mathbf{X}}_x^T \Sigma^{-1} \bar{\mathbf{X}}_x \right)^{-1} \bar{\mathbf{X}}_x^T \Sigma^{-1} \Delta\phi, \quad (9)$$

with $\bar{\mathbf{X}}_x = P_{\bar{\mathbf{X}}_x}^\perp \mathbf{X}_x$. The estimated position is filtered and transformed back to a phase tracking error which is then accumulated over time. Orthogonal projections can be derived in a similar way for the drifts of the receiver clock and atmospheric delays. The loop filters are adapted to the dynamics of the tracked parameters, and the tracked phases are recovered at the output of the MC-MS-VPLL.

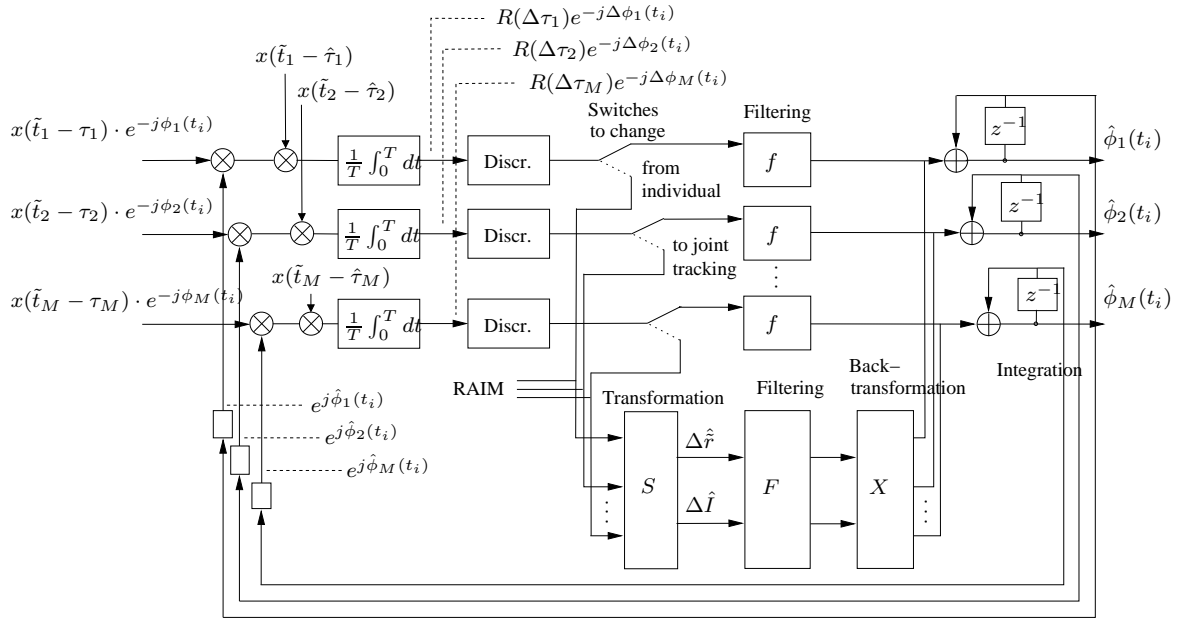


Fig. 1 Functional diagram of a Multi-Carrier, Single-Satellite Vector PLL: It is initialized by independent PLLs to avoid the estimation of integer ambiguities and biases. Once at least two PLLs are in lock, the tracking errors are transformed into a range drift and an ionospheric drift. Both parameters are filtered and transformed back to phase. The discriminator outputs are also used for RAIM to detect severe multipath and satellite anomalies.

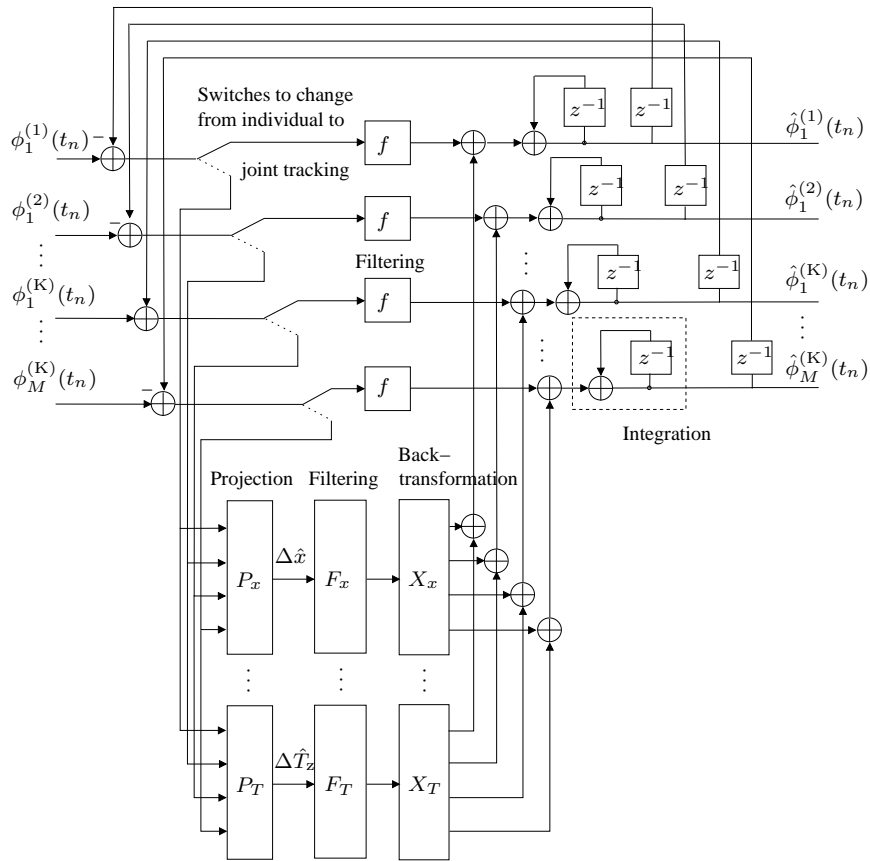


Fig. 2 Functional diagram of an extended Multi-Carrier, Multi-Satellite Vector PLL: Orthogonal projections are applied to the discriminator outputs to separate the drifts in position, receiver clock offset, ionospheric and tropospheric delays. The four loop filters are adapted to the dynamics of these parameters, and the phases of all satellites/ frequencies are recovered at the PLL output.

IMPACT OF IONOSPHERIC WIDEBAND EFFECTS ON CARRIER PHASE

The Galileo E5 signal has a bandwidth of 51 MHz which is more than 25 times the bandwidth of the GPS C/A code and results in a substantial reduction of the noise level. However, Gao et al. have shown in [4] that the ionospheric dispersion within wideband Galileo signals is not negligible. It causes ripples in the code signal that result in a power shift in correlation result from the real part to the imaginary part. If no wideband correction is applied, the phase tracked by an independent PLL is biased by $14^\circ/100$ TECU.

The dispersive ionosphere delays the transmitted baseband signal $s(t)$ which results in a phase shift in frequency domain. The distorted signal is obtained using the Fourier transform and its inverse, i.e.

$$\tilde{s}(t) = \int_{-\infty}^{+\infty} \int_{-\infty}^{+\infty} s(t) e^{-j2\pi ft} dt \cdot e^{-j2\pi f \cdot \tau(f)} \cdot e^{j2\pi ft} df, \quad (10)$$

with

$$\tau(f) = \frac{40.3 \cdot \text{TEC}}{f^2 \cdot c}, \quad (11)$$

where TEC represents the total electron content. In practice, measurements are sampled at $t = kT$ and the frequency is discretized to $f = f_0 + \frac{n}{NT}$ with the carrier frequency f_0 , the number of samples N , the sampling interval T and $n = [-\frac{N-1}{2}, \frac{N-1}{2}]$. Therefore, the time-continuous signal is replaced by a time-discrete signal and the DFT/IDFT are considered instead of the Fourier transform for continuous signals, i.e.

$$\begin{aligned} \tilde{s}[k] &= \frac{1}{N} \sum_{n=-\frac{N-1}{2}}^{\frac{N-1}{2}} \tilde{S}[n] \cdot e^{j2\pi \frac{kn}{N}} \\ &= \frac{1}{N} \sum_{n=-\frac{N-1}{2}}^{\frac{N-1}{2}} S[n] \cdot S_I[n] \cdot S_F[n] \cdot e^{j2\pi \frac{kn}{N}}, \end{aligned} \quad (12)$$

where $S[n]$ is the Fourier transform of the transmitted signal, i.e.

$$S[n] = \sum_{k=0}^{N-1} s[k] \cdot e^{-j2\pi \frac{kn}{N}} = \sum_{k=-\frac{N-1}{2}}^{\frac{N-1}{2}} s[k] \cdot e^{-j2\pi \frac{kn}{N}}, \quad (13)$$

and $S_I[n]$ is the Fourier transform of the ionospheric delay, i.e.

$$S_I[n] = \exp\left(-j2\pi \frac{n}{NT} \cdot \frac{40.3 \cdot \text{TEC}}{(f_0 + \frac{n}{NT})^2 \cdot c}\right), \quad (14)$$

and $S_F[n]$ is the Fourier transform of the low pass filter in the receiver, i.e.

$$S_F[n] = \begin{cases} 1 & \text{if } |\frac{n}{NT}| \leq \text{BW} \\ 0 & \text{else} \end{cases}, \quad (15)$$

with receiver bandwidth BW. Fig. 3 shows a functional diagram for the generation of wideband ionospheric effects.

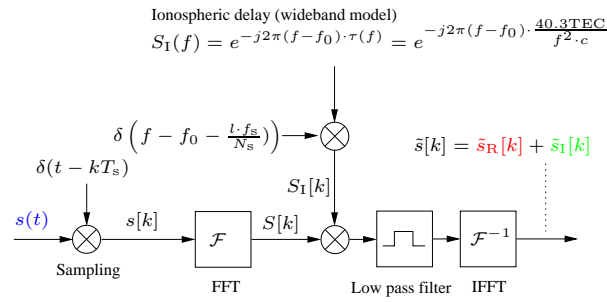
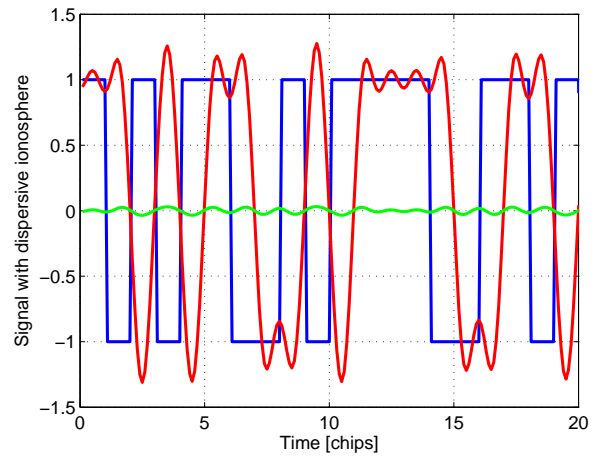
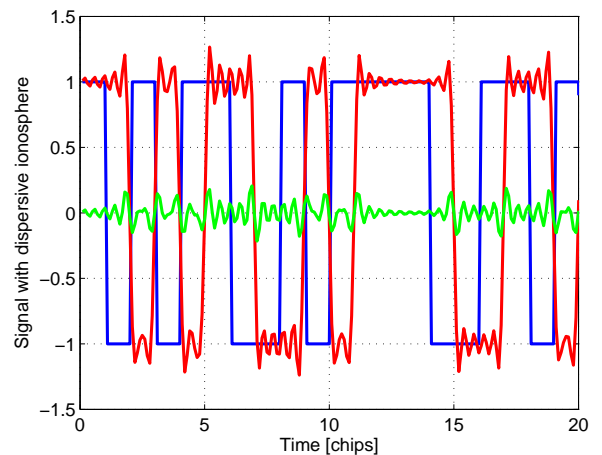


Fig. 3 Generation of wideband ionospheric effects: An individual phase shift is computed for each frequency.



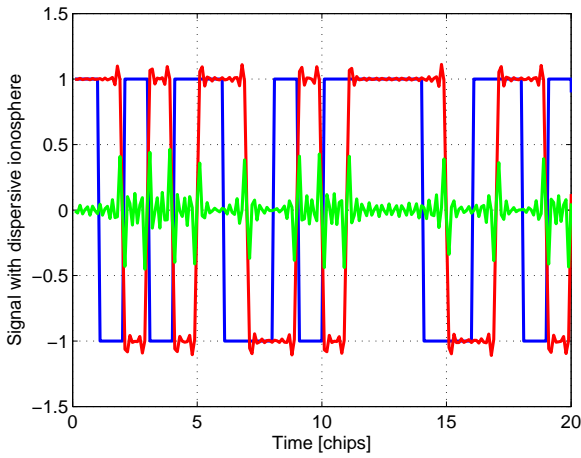
(a) E5a BPSK signal with 20 MHz bandwidth



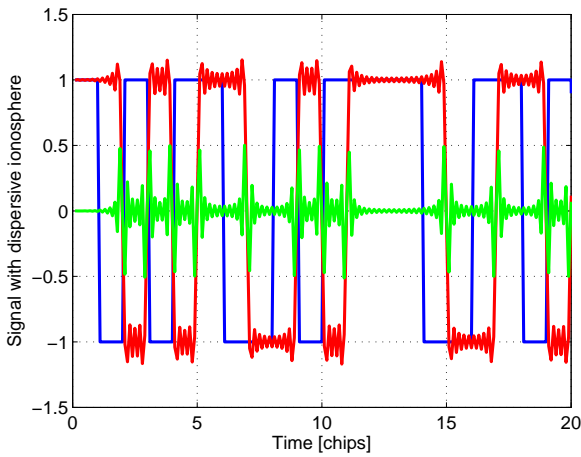
(b) E5a BPSK signal with 50 MHz bandwidth

Fig. 4 Signal distortion by wideband ionospheric effects (100 TEC) and different filter bandwidths.

Fig. 4 and 5 show the impact of the receiver bandwidth on the signal deformation of the BPSK modulated E5a signal. The signal that is not affected by the ionosphere is depicted as a reference in blue. The dispersive ionosphere delays the signal (100 TECU) and shifts some power from the real part (shown in red) to the imaginary part (shown in green). For $BW = 20$ MHz, the ripples due to the Gibb's phenomenon are dominating over the ripples due the ionospheric dispersion within the E5a band. The degradation of correlation and tracking results remains negligible for this modulation and bandwidth. Increasing the bandwidth reduces the Gibb's phenomenon but increases the ionospheric dispersion. For the real part of the signal, the smallest ripples can be observed for a bandwidth of 75 MHz. For the imaginary part of the signal, the amplitude of the ripples increases monotonously with the bandwidth.



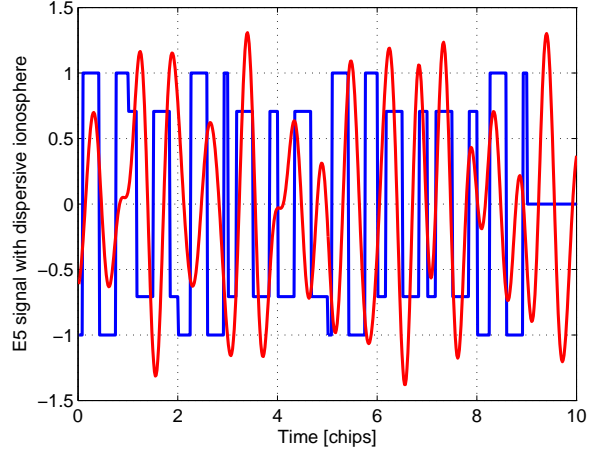
(a) E5a BPSK signal with 75 MHz bandwidth



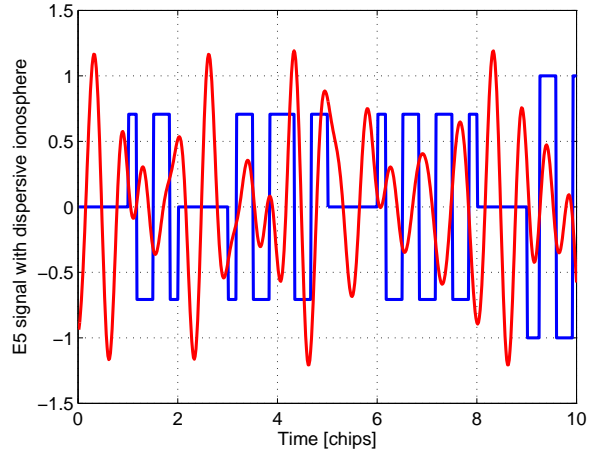
(b) E5a BPSK signal with 100 MHz bandwidth

Fig. 5 Signal distortion by wideband ionospheric effects (100 TEC) and different filter bandwidths: Increasing the bandwidth reduces the Gibb's phenomenon but increases the ionospheric dispersion.

Fig. 6 shows that the ionospheric dispersion is much more critical for the AltBOC E5 signal as a significant part of the power is allocated at the edges of the E5 band which has a bandwidth of 50 MHz.



(a) E5 AltBOC signal: real part



(b) E5 AltBOC signal: imaginary part

Fig. 6 Signal distortion by wideband ionospheric effects for 100 TECU: The degradation of the AltBOC signal is significantly stronger than of the BPSK(10) signals.

The Gibb's phenomenon is also more pronounced due to the use of a subcarrier which increases the number of chip transitions. Thus, the chips can no longer be recognized from the degraded signal shape.

The wideband ionosphere also degrades the correlation result which is obtained from Fig. 1 as

$$R(\Delta\tau_m) \cdot e^{-j\Delta\phi_m(t_i)}, \quad (16)$$

with the code correlation function

$$R(\Delta\tau_m) = \frac{1}{T_i} \int_0^{T_i} x(\tilde{t}_m - \tau_m) \cdot x(\tilde{t}_m - \hat{\tau}_m) d\tilde{t}_m, \quad (17)$$

where $\Delta\tau_m = \tau_m - \hat{\tau}_m$. The correlation function $R(\Delta\tau_m)$ is real-valued if there is no ionospheric dispersion within the band. For the GPS signals, $R(\Delta\tau_m)$ can be assumed real-valued as the intra-band ionospheric dispersion is negligible. Clearly, this is not the case for the wideband Galileo E5 signal which results in a complex correlation function that is written as

$$R(\Delta\tau_m) = R_{0,m} \cdot e^{j\Delta\tilde{\phi}_m(\Delta\tau_m)}. \quad (18)$$

As the discriminator can not distinguish between $\Delta\phi_m$ and $\Delta\tilde{\phi}_m$, the tracked phase is biased by $\Delta\tilde{\phi}_m(\Delta\tau_m)$. The code delay $\Delta\tau_m$ is determined such that the real part of the correlation result is maximized. Thus, the PLL tracking error is given by

$$\Delta\tilde{\phi}_m(\Delta\tau_{m,\max}) = \text{atan} \left(\frac{\Im(R(\Delta\tau_{m,\max}))}{\Re(R(\Delta\tau_{m,\max}))} \right) \quad (19)$$

with

$$\Delta\tau_{m,\max} = \arg \max_{\Delta\tau_m} \Re(R(\Delta\tau_m)). \quad (20)$$

Fig. 7a shows a reduced real-valued correlation peak for the AltBOC E5 signal as some part of the power is shifted from the real part to the imaginary part. Moreover, the correlation function is smoother compared to a non-dispersive ionospheric delay. The temporal shift of the correlation function corresponds to the ionospheric delay on the carrier frequency, i.e. the dispersion within the E5 band does not cause any additional delay for the code measurements.

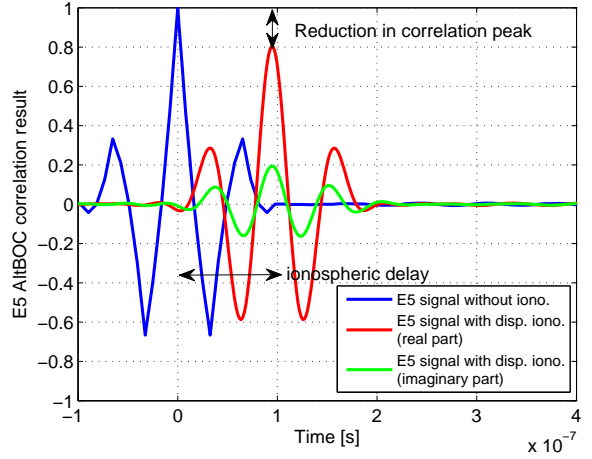
The maximum phase tracking error of Eq. (19) is shown for different TEC values and filter bandwidths in Fig. 7b. $\Delta\phi(\Delta\tau_{m,\max})$ increases linear with TEC but remains less than 0.5° for the E5a/E5b signals even during an active ionosphere. However, a phase offset of 15° can be observed for AltBOC(15,10) tracking during normal ionospheric conditions and of up to 70° during ionospheric storms.

COMPENSATION OF WIDEBAND IONOSPHERIC EFFECTS

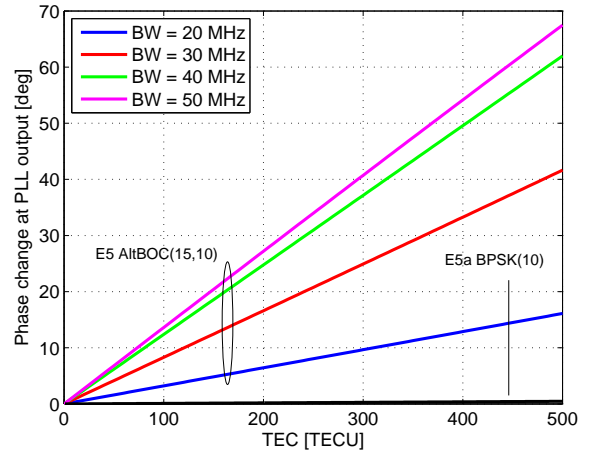
The correction of wideband ionospheric effects requires an estimate \hat{I} of the ionospheric delay that is not biased by wideband effects. As the intra-band ionospheric dispersion does not change the code delay, \hat{I} can be obtained by combining the E1 and E5 code measurements in a geometry-free, ionosphere-preserving linear combination. The received signal $\hat{s}[k]$ of Eq. (12) is corrected in frequency domain, i.e.

$$\hat{s}[k] = \mathcal{F}^{-1} (S_I^* \cdot \mathcal{F}(\hat{s}[k])), \quad (21)$$

where \mathcal{F} denotes the discrete Fourier transformation given by Eq. (13) and S_I^* is the conjugate complex of Eq. (14). An accuracy of 2 m for \hat{I} is sufficient to suppress the phase bias due to wideband ionospheric effects to less than 1° .



(a) E5 correlation result for 100 TECU



(b) Tracking error for different signal bandwidths

Fig. 7 Impact of wideband ionospheric effects on correlation and carrier tracking: The wideband ionosphere shifts some power from the real part to the imaginary part and smooths the correlation function. The phase change at the PLL output increases linear with TEC.

This method requires an FFT of the downconverted signal and an IFFT after the application of the wideband correction. Alternatively, a phase correction can be determined from a look-up table (e.g. Fig. 7b) and applied before tracking. The equalization in frequency domain is omitted, which improves the efficiency of this method as it does not require the FFT and IFFT.

INTEGRATION OF RAIM IN THE VECTOR PHASE LOCKED LOOP

Henkel, Giger and Günther have shown in [3] that the MC-MS-VPLL can substantially reduce the tracking errors of independent tracking loops. A drawback of the joint tracking of all satellites and frequencies is its susceptibility

to a failure on one satellite or frequency which also affects the tracking of all other satellites and frequencies. Therefore, the Weighted Receiver Autonomous Integrity Monitoring (RAIM) of Walter and Enge [5] shall be integrated into the VPLL for the detection and exclusion of measurements that are affected by satellite anomalies (e.g. phase jumps on satellite clocks) or severe multipath.

Fig. 8a shows the temporal evolution of the tracking error before and after a 90° phase jump on one satellite. This phase jump can not be mapped to the tracked position, clock offset or atmospheric delays. Therefore, an instability can be observed on all satellites after the phase jump. The assumed satellite geometry and the selected satellites are depicted in the skyplot. Another threat of the MC-MS-VPLL is an erroneous weighting matrix Σ . Fig. 8b shows a slight increase in the tracking error if the two satellites of lowest elevation are affected by a five times larger noise level than considered in Σ . However, the joint tracking still provides significantly lower tracking errors than independent PLLs during deep amplitude fades. Note that the temporal variations in the standard deviation of the tracking error are caused by strong ionospheric scintillations with an intensity index of $S_4 = 1.0$. Amplitude scintillations have been generated independently for each satellite. For a more detailed description of the implemented ionospheric scintillation model, the reader is referred to Pullen et al. [8]. Seo et al. have recently analyzed the characteristics of deep GPS signal fading due to ionospheric scintillations in [9].

In the VPLL of Fig. 1, the discriminator outputs provide the tracking errors $\Delta\phi = [\Delta\phi_1, \dots, \Delta\phi_M]^T$ that are used for RAIM. Weighted range residuals are evaluated to analyze the modeling accuracy of $\Delta\phi$ and to detect failures, i.e.

$$\mathbf{r} = (\mathbf{1} - \mathbf{X}(\mathbf{X}^T \Sigma^{-1} \mathbf{X})^{-1} \mathbf{X}^T \Sigma^{-1}) \Delta\phi, \quad (22)$$

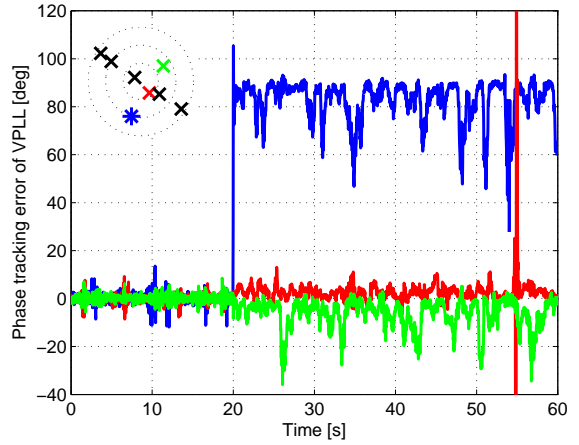
with \mathbf{X} given by Eq. (3). The range residuals are combined in a weighted sum of squared errors (WSSE) test statistic that is defined as

$$\text{WSSE} = \mathbf{r}^T \Sigma^{-1} \mathbf{r}, \quad (23)$$

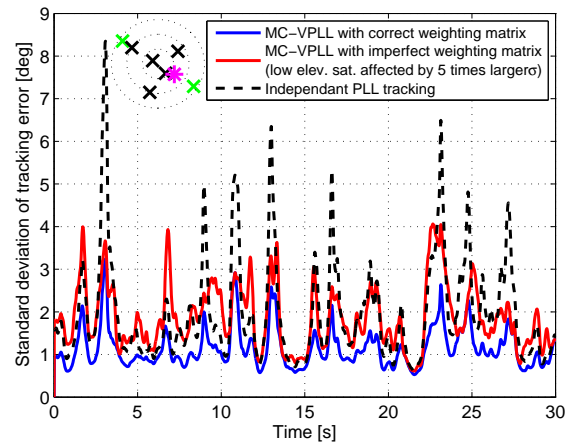
which can be rewritten as

$$\begin{aligned} \text{WSSE} &= \text{trace}(\mathbf{r}^T \Sigma^{-1} \mathbf{r}) \\ &= \text{trace}(\mathbf{r} \mathbf{r}^T \Sigma^{-1}) \\ &= \text{trace}\left(\left(\mathbf{1} - \mathbf{X}(\mathbf{X}^T \Sigma^{-1} \mathbf{X})^{-1} \mathbf{X}^T \Sigma^{-1}\right) \Delta\phi \right. \\ &\quad \left. \Delta\phi^T \left(\mathbf{1} - \mathbf{X}(\mathbf{X}^T \Sigma^{-1} \mathbf{X})^{-1} \mathbf{X}^T \Sigma^{-1}\right)^T \Sigma^{-1}\right) \end{aligned} \quad (24)$$

If $\Delta\phi$ can be modeled as in Eq. (2) and $\Delta\varepsilon \sim \mathcal{N}(\mathbf{0}, \Sigma)$, the WSSE is χ^2 distributed with $MK - 3 - 1 - K - 1 = (M - 1)K - 5$ degrees of freedom. The number of degrees of freedom is also the mean of the WSSE distribution.



(a) Phase jump on satellite clock



(b) Erroneous weighting matrix for VPLL

Fig. 8 Two threats of a MC-MS-VPLL: A sudden phase jump on one satellite results in an instability of the joint tracking. An erroneous weighting reduces the benefit of joint tracking but still benefits from lower tracking errors than individual PLLs.

An erroneous weighting matrix, phase jumps and severe multipath amplify the WSSE which motivates the introduction of the WSSE amplification factor, i.e.

$$A_{\text{WSSE}} = \frac{1}{(M - 1) \cdot K - 5} \cdot \text{WSSE}. \quad (25)$$

Fig. 9 shows how much σ_ϕ^k is scaled for a VPLL w.r.t. an independent PLL. The two satellites of lowest elevation are characterized by a standard deviation σ_ϕ that is γ times larger than considered in the weighting matrix. For $\gamma \leq 4.5$, the benefit of joint tracking is larger than the degradation due to a biased covariance matrix. If γ is increased beyond this threshold, more and more satellites are tracked with an error that is larger than in the case of independent PLLs. Fig. 9 also includes the WSSE amplification that increases faster with γ than σ_ϕ . The fault detecti-

on is based on a comparison between the WSSE and the threshold $WSSE_{th}$ that is given by the probability of false alarm $P_{FA} = P(WSSE(\gamma = 1) > WSSE_{th}) = 10^{-7}$. For a MC-MS-VPLL with $M = 3$ and $K = 8$, there exist 11 degrees of freedom which results in the threshold $WSSE_{th} = 54.4$. The WSSE exceeds this threshold with a probability of 45.5% for $\gamma = 5$, of 77.9% for $\gamma = 7.5$, and of 90.9% for $\gamma = 10$.

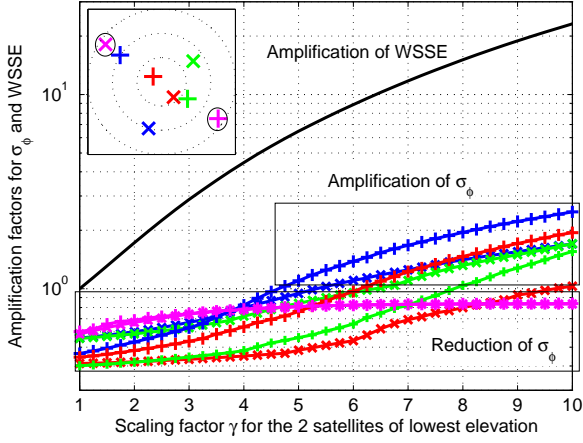


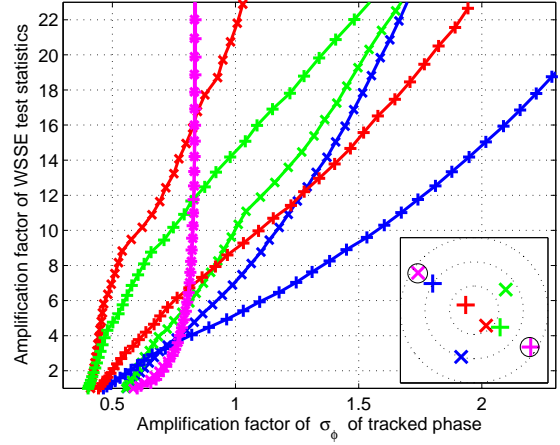
Fig. 9 Detection of erroneous weighting matrix from WSSE amplification: For $\gamma \leq 4.5$, the benefit of joint tracking is still larger than the degradation due to an erroneous weighting.

Fig. 10 shows the WSSE amplification as a function of the scaling of σ_{ϕ} . In the upper subfigure, the two satellites of lowest elevation are affected by $\gamma \in [1, 10]$ and, in the lower subfigure, the two satellites of highest elevation suffer from an enhanced noise level. In both cases, the WSSE amplification exceeds the σ_{ϕ} amplification and tends to be larger for high elevation satellites than for low elevation satellites. Note that the σ_{ϕ} amplification of the critical satellites converges to a certain value as the scaling of γ affects both the MC-MS-VPLL and the independent PLL.

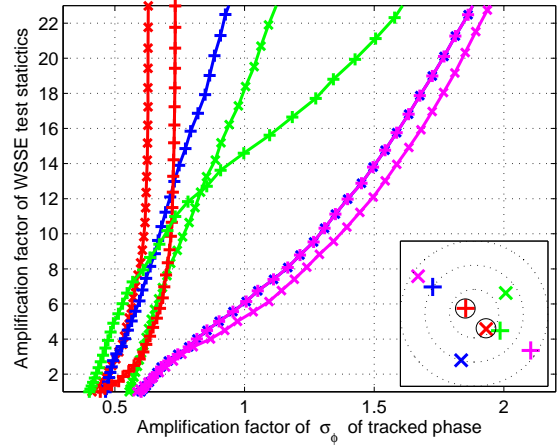
The WSSE test statistic is also used to detect carrier phase multipath. In [10], Georgiadou and Kleusberg have determined the phase bias due to multipath from multiple reflections for a baseline of 24 m: They computed the geometry-free $\lambda_1\phi_1 - \lambda_2\phi_2$ linear combination and subtracted the mean of this linear combination to eliminate the integer ambiguities. They repeated this experiment on the next day at the same time and observed an impressive correlation between both geometry-free combinations. Their model for multipath with multiple reflections is briefly introduced here and then used for the MC-MS-VPLL. The sum of the direct and all reflected signals is described by

$$s = A \cos(\phi) + A \sum_{i=1}^{n_r} \alpha_i \cos(\phi + \theta_i), \quad (26)$$

with the amplitude A and phase ϕ of the direct signal, the



(a) Erroneous weighting of low elev. sat.



(b) Erroneous weighting of high elev. sat.

Fig. 10 Detection of erroneous weighting matrix from WSSE amplification: The WSSE increases much faster than σ_{ϕ} if the error in the weighting is increased.

fading coefficient α_i and the phase offset θ_i of the i -th reflected path. Equation (26) can also be written as

$$s = A\beta \cos(\phi + \psi), \quad (27)$$

with

$$\beta = \sqrt{\left(1 + \sum_{i=1}^{n_r} \alpha_i \cos(\theta_i)\right)^2 + \left(\sum_{i=1}^{n_r} \alpha_i \sin(\theta_i)\right)^2} \quad (28)$$

and

$$\psi = \arctan\left(\frac{\sum_{i=1}^{n_r} \alpha_i \sin(\theta_i)}{1 + \sum_{i=1}^{n_r} \alpha_i \cos(\theta_i)}\right). \quad (29)$$

Fig. 11 shows the WSSE amplification for a dual frequency (E1-E5a) MC-MS-VPLL during strong multipath from

a single reflector. It is assumed that only the two satellites of lowest elevation are affected by multipath on both frequencies but all satellites are affected by severe ionospheric scintillations ($S_4 = 1.0$).

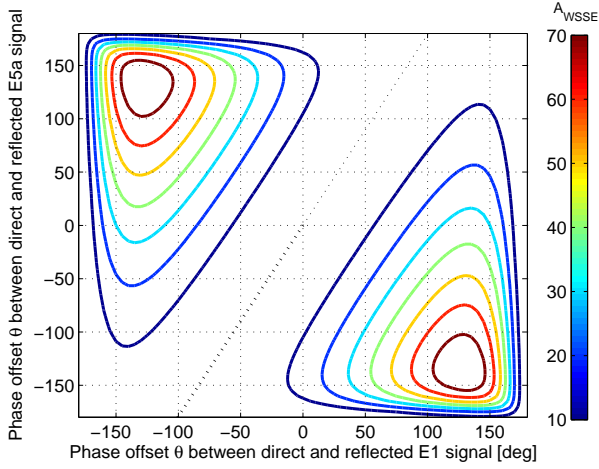


Fig. 11 Detection of carrier phase multipath ($\alpha_i = 0.9$) from WSSE amplification during severe ionospheric scintillations ($S_4 = 1.0$): Phase offsets that result in large WSSE amplification can be easily detected. If the multipath induced delays show the same behaviour as the ionospheric delays, no WSSE amplification is observed and the joint tracking is not deteriorated.

The WSSE amplification is negligible for the phase offsets $\theta = \pm\pi$ which result in a power loss but no phase bias. A low power turns into a low weight in the MC-MS-VPLL which compensates these power fades with the help of other satellites and frequencies. No WSSE amplification is also observed if $\theta_{E5} = f_{E1}^2/f_{E5}^2 \cdot \theta_{E1}$. In this case, the multipath is mapped to the ionospheric delay which is a tracked parameter and does not cause a WSSE amplification. The largest WSSE occurs for $\theta_{E5} = \pm 130^\circ$ and $\theta_{E5} = -\theta_{E1}$, which corresponds to a phase offset of 90° between both reflections. However, such a multipath is also not critical as it can be easily detected from the large WSSE amplification. The reliability of multipath detection becomes critical only for $A_{WSSE} < 10$. The fault detection capability improves for less intense ionospheric scintillations due to the reduced number of deep amplitude fades.

RAIM WITH MULTIPLE FAULTS

Multipath can affect the tracking of multiple satellites and requires fault detection in the MC-MS-VPLL. Walter and Enge have derived protection levels for single satellite failures in [5] and Angus has generalized this approach to multiple faults in [11]. His approach is briefly introduced and then applied to the carrier tracking errors that are provided by the phase discriminators. The $MK \times 1$ bias

vector \mathbf{b} is written as

$$\mathbf{b} = \mathbf{Q}\mathbf{b}^*, \quad (30)$$

where \mathbf{b}^* denotes an $r \times 1$ non-zero bias vector and \mathbf{Q} is an $MK \times r$ matrix that maps the non-zero bias values to the measurements. The most critical bias vector maximizes the position bias under the constraint that the test statistic does not exceed the threshold $WSSE_{th}$, i.e.

$$\max_{\mathbf{Q} \in \mathcal{Q}_r} \max_{\mathbf{b}^*, \mathbf{b}^{*T} \mathbf{Q}^T \mathbf{S} \mathbf{Q} \mathbf{b}^* = WSSE_{th}} \sqrt{\mathbf{b}^{*T} \mathbf{Q}^T \mathbf{D} \mathbf{Q} \mathbf{b}^*}, \quad (31)$$

which also maximizes the square of the horizontal or vertical position bias. If the horizontal direction is chosen, \mathbf{D} is given by

$$\begin{aligned} D_H &= \Sigma^{-1} \mathbf{X} \left(\mathbf{X}^T \Sigma^{-1} \mathbf{X} \right)^{-1} \mathbf{P}_h^T \\ &\quad \mathbf{P}_h \left(\mathbf{X}^T \Sigma^{-1} \mathbf{X} \right)^{-1} \mathbf{X}^T \Sigma^{-1} \end{aligned} \quad (32)$$

with $\mathbf{P}_h = [\mathbf{1}^{2 \times 2}, \mathbf{0}^{2 \times 3+K}]$. The maximum vertical bias is obtained similarly as

$$\begin{aligned} D_V &= \Sigma^{-1} \mathbf{X} \left(\mathbf{X}^T \Sigma^{-1} \mathbf{X} \right)^{-1} \mathbf{P}_v^T \\ &\quad \mathbf{P}_v \left(\mathbf{X}^T \Sigma^{-1} \mathbf{X} \right)^{-1} \mathbf{X}^T \Sigma^{-1} \end{aligned} \quad (33)$$

with $\mathbf{P}_v = [0, 0, 1, \mathbf{0}^{1 \times 2+K}]$. The optimization of (31) is an eigenvalue problem which can also be expressed as

$$\max_{\mathbf{x} \neq \mathbf{0}} \frac{\mathbf{x}^T \mathbf{A} \mathbf{x}}{\mathbf{x}^T \mathbf{x}} = \lambda_{\max}, \quad (34)$$

where λ_{\max} is the largest eigenvalue of \mathbf{A} that is given by

$$\mathbf{A} = \mathbf{Q}^T \mathbf{D} \mathbf{Q} \left(\mathbf{Q}^T \mathbf{S} \mathbf{Q} \right)^{-1}. \quad (35)$$

The position biases $\sqrt{\lambda_{\max}}$ are included in the protection levels that are given by Angus as

$$\begin{aligned} \text{HPL} &= \max_{\mathbf{Q} \in \mathcal{Q}_r} \sqrt{\lambda_{\max}(\mathbf{D}_h, \mathbf{Q}, \mathbf{S}) \cdot WSSE_{th}} \\ &\quad + k_h \cdot \left(\left[\left(\mathbf{X}^T \Sigma^{-1} \mathbf{X} \right)^{-1} \right]_{1,1} \right. \\ &\quad \left. + \left[\left(\mathbf{X}^T \Sigma^{-1} \mathbf{X} \right)^{-1} \right]_{2,2} \right)^{1/2}, \end{aligned} \quad (36)$$

and

$$\begin{aligned} \text{VPL} &= \max_{\mathbf{Q} \in \mathcal{Q}_r} \sqrt{\lambda_{\max}(\mathbf{D}_v, \mathbf{Q}, \mathbf{S}) \cdot WSSE_{th}} \\ &\quad + k_v \cdot \sqrt{\left[\left(\mathbf{X}^T \Sigma^{-1} \mathbf{X} \right)^{-1} \right]_{3,3}}. \end{aligned} \quad (37)$$

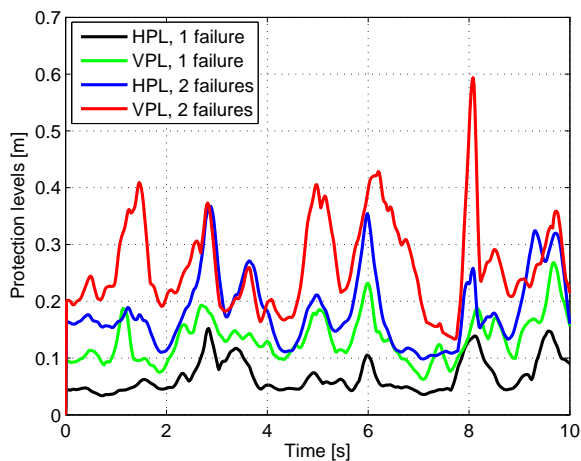


Fig. 12 Protection levels based on carrier tracking errors of the discriminator outputs for a probability of false alert of 10^{-6} : The temporal variations are caused by strong ionospheric scintillations with $S_4 = 1.0$. In addition, two satellite failures can be protected with a protection level of at most 60 cm.

Fig. 12 shows the horizontal and vertical protection levels for a triple frequency MC-MS-VPLL that tracks the position, the receiver clock offset, the ionospheric and tropospheric delays. The same geometry has been considered as in Fig. 8-10. The covariance matrix is computed from the standard deviations of the carrier tracking errors at the discriminator outputs. A VPL of at most 30 cm is observed for single failures and of up to 60cm for two failures during severe ionospheric scintillations with $S_4 = 1.0$.

CONCLUSIONS

A multi-carrier, multi-satellite vector phase locked loop couples the individual tracking loops by performing the filtering in position domain. The drifts in position, clock offset, ionospheric and tropospheric delays are obtained from the tracking errors by weighted least-square estimation. The joint tracking reduces the tracking errors efficiently as the stronger signals help to track the weaker ones.

In this paper, two extensions have been proposed for the vector phase locked loop: The first one is a correction of wideband ionospheric effects that can result in phase biases of up to 70° for the wideband Galileo E5 signal. The second one is the integration of a weighted RAIM for the detection and exclusion of biased measurements from the joint tracking. Both extensions are recommended to benefit from the advantages of joint tracking.

REFERENCES

- [1] J. Spilker, Fundamentals of Signal Tracking Theory, *Global Positioning System: Theory and Application Volume I*, edited by B. Parkinson and J. Spilker, Progress in Aeronautics and Astronautics, Volume 163, 1996.
- [2] M. Zhodzishsky, S. Yudanov, V. Veitsel and J. Ashjaee, Co-Op Tracking for carrier phase, *Proc. of ION-GPS '98*, pp. 653-664, Nashville (TN), USA, Sep. 1998, also U.S. patent (6.313.789 B1), June 1998.
- [3] P. Henkel, K. Giger and C. Günther, Multi-Carrier Vector Phase Locked Loop for Robust Carrier Tracking, *Proc. of European Navigation Conference (ENC)*, Toulouse, France, Apr. 2008.
- [4] G. Gao, S. Datta-Barua, T. Walter and P. Enge, Ionospheric Effects for Wideband GNSS Signals, *ION Annual Meeting*, Cambridge (MA), USA, Apr. 2007.
- [5] T. Walter and P. Enge, Weighted RAIM for Precision Approach, *Proc. of the 8th International Technical Meeting of the Institute of Navigation*, Palm Springs, CA, pp. 1995-2004, Sep. 1995.
- [6] E. Kaplan and C. Hegarty, Understanding GPS - Principles and applications, 2nd edition, *Artech House*, 2006.
- [7] P. Teunissen, Adjustment theory - an introduction, *Series on Mathematical Geodesy and Positioning*, TU Delft, 2003.
- [8] S. Pullen, G. Opshaug, A. Hansen, T. Walter, P. Enge and B. Parkinson, A Preliminary Study of the Effect of Ionospheric Scintillation on WAAS User Availability in Equatorial Regions, *Proc. of ION-GPS '98*, pp. 687-699, Nashville, TN, Sep. 1998.
- [9] J. Seo, T. Walter, T.-Y. Chiou and P. Enge, Characteristics of Deep GPS Signal Fading Due to Ionospheric Scintillation for Aviation Receiver Design, *Radio Science*, doi:10.1029/2008RS004077, in press, 2009.
- [10] Y. Georgiadou and A. Kleusberg, On carrier signal multipath effects in relative GPS positioning, *Manuscripta geodetica*, Springer Verlag, Vol. 13, pp. 172-179, 1988.
- [11] J. Angus, RAIM with Multiple Faults, *Journal of the Institute of Navigation*, Vol. 53, No. 4, pp. 249-257, Winter 2006.